

## Molecular Basis for Atovaquone Binding to the Cytochrome $bc_1$ Complex\*

Received for publication, April 17, 2003, and in revised form, June 3, 2003  
Published, JBC Papers in Press, June 5, 2003, DOI 10.1074/jbc.M304042200

Jacques J. Kessler<sup>‡</sup>, Benjamin B. Lange<sup>‡</sup>, Torsten Merbitz-Zahradnik<sup>‡</sup>, Klaus Zwicker<sup>§</sup>,  
Philip Hill<sup>¶</sup>, Brigitte Meunier<sup>¶</sup>, Hildur Pálsdóttir<sup>¶</sup>, Carola Hunte<sup>¶</sup>, Steve Meshnick<sup>\*\*</sup>,  
and Bernard L. Trumpower<sup>‡</sup> <sup>‡‡</sup>

From the <sup>‡</sup>Department of Biochemistry, Dartmouth Medical School, Hanover, New Hampshire 03755, <sup>§</sup>Universitätsklinikum Frankfurt, ZBC, Biochemie I, D-60590 Frankfurt, Germany, the <sup>¶</sup>Wolfson Institute for Biomedical Research, University College London, London WC1E6BT, United Kingdom, <sup>¶</sup>Max-Planck-Institut für Biophysik, Marie-Curie-Strasse 15, D-60439 Frankfurt, Germany, and the <sup>\*\*</sup>Department of Microbiology and Immunology, University of North Carolina, Chapel Hill, North Carolina 27599

Atovaquone is a substituted 2-hydroxynaphthoquinone that is used therapeutically to treat *Plasmodium falciparum* malaria, *Pneumocystis carinii* pneumonia, and *Toxoplasma gondii* toxoplasmosis. It is thought to act on these organisms by inhibiting the cytochrome  $bc_1$  complex. We have examined the interaction of atovaquone with the  $bc_1$  complex isolated from *Saccharomyces cerevisiae*, a surrogate, nonpathogenic fungus. Atovaquone inhibits the  $bc_1$  complex competitively with apparent  $K_i = 9$  nM, raises the midpoint potential of the Rieske iron-sulfur protein from 285 to 385 mV, and shifts the g values in the EPR spectrum of the Rieske center. These results indicate that atovaquone binds to the ubiquinol oxidation pocket of the  $bc_1$  complex, where it interacts with the Rieske iron-sulfur protein. A computed energy-minimized structure for atovaquone liganded to the yeast  $bc_1$  complex suggests that a phenylalanine at position 275 of cytochrome *b* in the bovine  $bc_1$  complex, as opposed to leucine at the equivalent position in the yeast enzyme, is responsible for the decreased sensitivity of the bovine  $bc_1$  complex ( $K_i = 80$  nM) to atovaquone. When a L275F mutation was introduced into the yeast cytochrome *b*, the sensitivity of the yeast enzyme to atovaquone decreased ( $K_i = 100$  nM) with no loss in activity, confirming that the L275F exchange contributes to the differential sensitivity of these two species to atovaquone. These results provide the first molecular description of how atovaquone binds to the  $bc_1$  complex and explain the differential inhibition of the fungal versus mammalian enzymes.

The cytochrome  $bc_1$  complex (EC 1.10.2.2) is an essential respiratory enzyme complex present in the inner mitochondrial membrane of eukaryotic organisms. The  $bc_1$  complex catalyzes electron transfer from ubiquinol to cytochrome *c* and concomitantly translocates protons across membranes (1). The enzyme

is a functional dimer, with variable subunit composition among species. The essential subunits for electron transfer and energy transduction are those that contain prosthetic groups, cytochrome *b*, cytochrome  $c_1$ , and the Rieske iron-sulfur protein.

Atovaquone (2-[trans-4-(4'-chlorophenyl)cyclohexyl]-3-hydroxy-1,4-hydroxynaphthoquinone) (2, 3) is an anti-protozoal compound that has broad-spectrum activity against apicomplexan parasites including *Plasmodium* (4), *Toxoplasma* (5), *Theileria* (6), and *Babesia* (7) and the fungus *Pneumocystis carinii* (8). The effects of the drug on cell respiration and the structural similarities of atovaquone and ubiquinol suggested that the  $bc_1$  complex was the target (4). This has been supported by the emergence of mutations in the cytochrome *b* gene coincident with resistance to the drug (9–14). Because of the appearance of atovaquone resistance in these protozoan parasites, the mechanism of binding of the drug to the  $bc_1$  complex must be fully understood in order to improve its effectiveness. However, to date there has been no characterization of the interaction of atovaquone with the isolated enzyme.

We have been developing *Saccharomyces cerevisiae* as a surrogate organism in which to model the mechanism of atovaquone action in the above named pathogens. This yeast was chosen for these studies because of the high sequence identity between its cytochrome *b* and those of *Plasmodium* and *P. carinii* (15). In addition, the yeast enzyme can easily be purified, and its crystal structure is available (16).

In the current study, we have characterized the interaction of atovaquone with the yeast cytochrome  $bc_1$  complex. Based on these results, we have developed a model that describes the molecular basis for atovaquone binding at the ubiquinol oxidation pocket of the  $bc_1$  complex. This model also explains the basis for the differential efficacy of inhibition of the yeast and bovine  $bc_1$  complexes by atovaquone.

### EXPERIMENTAL PROCEDURES

**Materials**—Yeast extract and peptone were from Difco. Nitrogen base without amino acids but with ammonium sulfate was from U.S. Biological. Dodecylmaltoside was obtained from Roche Applied Science. DEAE-Biogel A was obtained from Bio-Rad. Diisopropylfluorophosphate, decyl ubiquinone, and dithionite were purchased from Sigma. Stigmatellin was purchased from Fluka Biochemica. Atovaquone was a gift from Glaxo-Wellcome.

**Purification of Cytochrome  $bc_1$  Complexes**—Wild type yeast and the L275F mutant were grown in yeast extract/peptone/dextrose medium and harvested by centrifugation. The L275F mutation was introduced into the mitochondrial cytochrome *b* gene by biolistic transformation as described elsewhere (15). Cytochrome  $bc_1$  complexes were isolated from yeast and bovine heart mitochondria as described previously (17, 18)

\* This work was supported by National Institutes of Health Grants GM 20379 (to B. L. T.) and AI46966 (to S. M.), Deutsche Forschungsgemeinschaft Grant SFB 472 (to C. H.), a Medical Research Fellowship (to B. M.), and a Biotechnology and Biological Sciences Research Council Studentship (to P. H.). The costs of publication of this article were defrayed in part by the payment of page charges. This article must therefore be hereby marked "advertisement" in accordance with 18 U.S.C. Section 1734 solely to indicate this fact.

<sup>‡‡</sup> To whom correspondence should be addressed: Dept. of Biochemistry, Dartmouth Medical School, 7200 Vail Bldg., Hanover, NH 03755. Tel.: 603-650-1621; Fax: 603-650-1389; E-mail: Trumpower@Dartmouth.edu.

and concentrated by centrifugal filtration, using Amicon® Centriprep YM-30 filtration tubes.

**Ubiquinol-Cytochrome *c* Reductase Activity Measurements**—Cytochrome *c* reductase activity was assayed in 50 mM potassium phosphate, pH 7.0, 250 mM sucrose, 0.2 mM EDTA, 1 mM Na<sub>2</sub>N<sub>3</sub>, 2.5 mM KCN, 0.01% Tween 20, and 40 μM cytochrome *c* at 23 °C. The cytochrome *bc*<sub>1</sub> complex was diluted to 2.5 nM in the assay buffer, and the reaction was started by adding 2,3-dimethoxy-5-methyl-6-decyl-1,4-benzoquinol, an analogue of ubiquinol. To determine activities in the presence of various concentrations of atovaquone, inhibitor and substrate were mixed simultaneously into the assay buffer, and the reaction was started by adding enzyme. Reduction of cytochrome *c* was monitored in an Aminco DW-2a spectrophotometer at 550 versus 539 nm in dual wavelength mode. Data were collected and analyzed using an Online Instrument Systems Inc. computer interface and software. Assuming rapid equilibrium between enzyme, substrate, and inhibitor, the *K<sub>i</sub>* values for a competitive inhibitor were calculated from the measured IC<sub>50</sub> values and the following formula (19).

$$K_i = \frac{IC_{50}}{1 + \frac{[S]}{K_m}} \quad (\text{Eq. 1})$$

**EPR<sup>1</sup> Spectroscopy**—EPR spectra were recorded at a temperature of 20 K, microwave frequency of 9.47 GHz, microwave power of 1 milliwatt, and a modulation amplitude of 0.64 millitesla using a Bruker ESP 300E spectrometer equipped with a liquid helium continuous flow cryostat, ESR 900, from Oxford Instruments. The *bc*<sub>1</sub> complex was diluted to 24 μM in a buffer containing 250 mM sucrose, 50 mM potassium phosphate, 1 mM sodium azide, 0.2 mM EDTA, and 0.01% Tween 20, pH 7.0. The samples were reduced with 5 mM ascorbate. After reduction, 3 eq of atovaquone (72 μM) or stigmatellin were added when indicated, and the samples were incubated for 20 min on ice. For base-line correction, a sample of *bc*<sub>1</sub> complex without any addition, representing the oxidized state, was subtracted from the spectra of ascorbate-reduced samples. We estimate that the deviations in *g<sub>x</sub>* and *g<sub>y</sub>* are ±0.001, and those in *g<sub>z</sub>* are ±0.005 in the spectra shown.

**Potentiometric Titrations**—The titrations were performed by CD spectroscopy in an OTTLE cell with a path length of 100 μm (20). The concentration of *bc*<sub>1</sub> complex was at least 300 μM. A mixture of redox mediators including benzyl viologen (−358 mV), anthraquinone-2-sulfonate (−225 mV), 2-hydroxy-1,4-naphthoquinone (−152 mV), menadiolone (−13 mV), duroquinone (5 mV), phenazine ethosulfate (55 mV), phenazine methosulfate (80 mV), trimethyl-1,4-benzoquinone (99 mV), 1,2-naphthoquinone (144 mV), tetramethyl-*p*-phenyldiamine (276 mV), potassium hexacyanoferrate (408 mV), and ferrocene-1,1'-dicarboxylic acid (530 and 644 mV) was added to facilitate equilibration with the electrode potentials (numbers in brackets are *E<sub>m,7</sub>* of the mediators in mV). The mediators, which spanned the potential range from −358 to +644 mV, were all present at a final concentration of 20–25 μM. Equilibration of the protein with the applied potential was confirmed by repetitive scan monitoring of the redox state of the entire *bc*<sub>1</sub> complex. Only spectra of the completely equilibrated protein were used for data analysis. The inhibitors NHDBT and atovaquone were added in 3-fold molar excess. Four scans of the spectrum at each potential value were accumulated with a scan speed of 200 nm/min, 2-nm bandwidth, and an integration time of 4 s. From the resulting spectrum, the amplitudes of the CD signal at five wavelengths (494, 498, 500, 502, and 505 nm) centering around 500 nm were extracted from each spectrum, and the amplitude values were averaged. This wavelength was chosen to monitor the potentiometric titration, since the reduced iron-sulfur protein has a CD signal centering around 500 nm that disappears when the cluster is oxidized (for an example of the reduced protein spectrum, see Ref. 20). From the total amplitude change, the degree of reduction of the Rieske protein was calculated. Complete reduction refers to the negative CD signal intensity of the Rieske protein. The amplitudes of the CD signals at 500 nm are indicated in the legend to Fig. 4. The potential curves were fitted by Nernstian functions assuming an *n* = 1 electron transition.

**Molecular Modeling**—Atovaquone was built *in silico* and an energy-minimized conformation was calculated using MacSpartan Pro® (Wavefunction, Inc., Irvine, CA). The initial structure was submitted to

a conformational energy profile determination by molecular mechanics using the MMFF function in the program. The lowest energy conformer was then submitted to a more refined energy minimization in the same program using the Hartree-Fock molecular orbital method and a 3–21 G basis set for the calculation. The theoretical basis of the molecular mechanics calculations using the MMFF force field and the Hartree-Fock quantum mechanical calculations, including a description of the 3–21 G split valence basis set, is described elsewhere (21). The energy-minimized conformation of atovaquone thus obtained was used as a starting point for modeling the ligand into the yeast cytochrome *bc*<sub>1</sub> complex.

Molecular modeling was carried out on a Silicon Graphics O2 workstation using the Discover 3® module within the Insight II® software package (Accelrys Inc., San Diego, CA). The starting structure was the stigmatellin-ligated yeast cytochrome *bc*<sub>1</sub> complex (Protein Data Bank code 1EZV) at a resolution of 2.30 Å (16). Atovaquone and cytochrome *b* residues within 4.0 Å of either atovaquone or Glu<sup>272</sup> were allowed to be flexible. A surrounding 9.5-Å shell of residues in both cytochrome *b* and the iron-sulfur protein was fixed, and the most distant residues were excluded from the calculation in order to obtain a manageable simulation speed. A 9.5-Å atom-based cut-off for nonbonding interactions was used during the calculations, with the dielectric constant set at 2.0. Eight simulated annealing runs were performed, each from 800 to 298 K, with five temperature steps and a simulation time of 5000 fs/step. The Nosé temperature control method (22) was used with a 0.5 fs/iteration time step.

A custom macro was written to select the lowest energy structure from each dynamics run for continued modeling. Between each dynamics run, a minimization of 250 iterations was performed. After the final round of molecular dynamics, the lowest energy structure was minimized to a final convergence criterion of 0.001, using Cauchy's steepest descent method as implemented in the Discover 3® module within the Insight II® software, followed by conjugate gradient (23), and Newton (Broyden, Fletcher, Goldfarb, and Shand) methods (24) in succession. Of the eight minimized results obtained, the three lowest energy structures were chosen, and each was modeled again twice, using the same set of parameters. Overlaying the final atovaquone-bound structure on the original stigmatellin structure showed a minimal amount of backbone shifting and, with the exception of the rotated Glu<sup>272</sup> side chain, just enough side-chain movement to accommodate the chloro-benzyl tail of atovaquone.

The cytochrome *b* mutation L275F was built into the modeled atovaquone-bound center P site using the Biopolymer® module. The flexible subset was defined by a 2.0-Å radius from the mutated residue L275F. A 9.5-Å surrounding radius, including atovaquone, was kept fixed. This minimal flexibility allowed evaluation of the energy cost that the L275F mutation has on atovaquone binding. Using the same procedure as for the modeling of atovaquone into the wild-type structure, four simulated annealing runs were carried out on the L275F mutant structure. The final energy of each of the four L275F mutant runs was evaluated using the CFF91 force field and the same residues as for the wild-type runs.

## RESULTS

**Structural Similarities between Atovaquone and Stigmatellin**—Stigmatellin (25) is a competitive inhibitor (26) that binds in the ubiquinol oxidation pocket at center P of the *bc*<sub>1</sub> complex. Its benzopyranone ring system binds to the yeast *bc*<sub>1</sub> complex via its hydroxyl group to Glu<sup>272</sup> of cytochrome *b* and via its carbonyl group to His<sup>181</sup> of the Rieske iron-sulfur protein (16). Atovaquone also inhibits the *bc*<sub>1</sub> complex and, by analogy to other hydroxyquinone inhibitors (27), is presumed to bind to the ubiquinol oxidation pocket. Below, we show that this presumption is correct and that, like stigmatellin, atovaquone is a competitive inhibitor of the enzyme. The structural basis for stigmatellin binding to the yeast *bc*<sub>1</sub> complex is thus a useful starting point to elucidate the structural basis of atovaquone binding.

In Fig. 1, we have compared the energy-minimized structure of atovaquone with the structure of stigmatellin extracted from the yeast *bc*<sub>1</sub> complex with stigmatellin bound (Protein Data Bank code 1EZV). The energy-minimized structure of atovaquone is one in which the hydroxynaphthoquinone and chlorophenyl rings are rotated 90° relative to the cyclohexyl ring that links them, and the latter is in a chair conformation. When the

<sup>1</sup> The abbreviations used are: EPR, electron paramagnetic resonance; OTTLE, optically transparent thin layer electrode; UHDBT, 3-undecyl-2-hydroxy-1,4-benzoxothiazole; HDBT, 2-hydroxy-1,4-benzoxothiazole; NHDBT, 3-nonyl-2-hydroxy-1,4-benzoxothiazole.

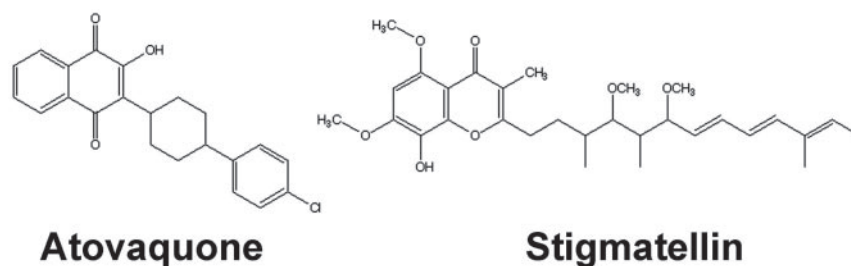
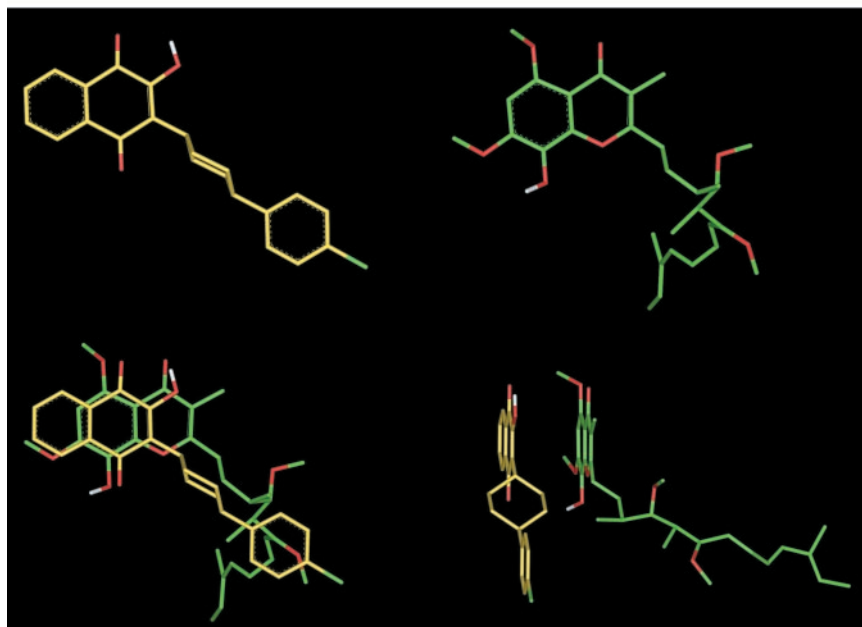


**FIG. 1. Structures of atovaquone and stigmatellin.** The structures of the two inhibitors are shown at the top. Below, in color, are shown the energy-minimized conformation of atovaquone (in yellow) and the structure of stigmatellin (in green) as it appears in the yeast crystal structure (Protein Data Bank code 1EZV). At the bottom, the two inhibitors are superimposed and shown in two views, rotated  $\sim 90^\circ$  with respect to each other.



calculated atovaquone structure is superposed on the stigmatellin structure, the two inhibitors display structural similarities in the alignment of their ring systems (Fig. 1). This is one indication that the two molecules probably share the same binding mode on the  $bc_1$  complex. Although there is some structural similarity between the hydroxyquinone ring of atovaquone and the benzopyranone of stigmatellin, the side chains extending from the rings differ significantly, both in structure and in spatial conformation.

**Atovaquone Is a Competitive Inhibitor of the  $bc_1$  Complex**—Inhibition by atovaquone was measured, and the type of inhibition was determined using cytochrome  $bc_1$  complex purified from the yeast. The results from this characterization are shown in Fig. 2. Under the usual conditions of a cytochrome  $c$  reductase assay, with enzyme and substrate concentrations of 2.5 nM and 50  $\mu$ M, respectively, titration of the inhibitor results in an  $IC_{50} = 50$  nM. From the reciprocal plots of initial velocity versus substrate concentration at different atovaquone concentrations, it is evident that the compound is a competitive inhibitor of the enzyme. Using a value of 11  $\mu$ M determined for the  $K_m$  in the absence of inhibitor, one can calculate an apparent  $K_i = 9$  nM for the competitive inhibitor.

**Interaction of Atovaquone with the Rieske Iron-Sulfur Protein**—Stigmatellin and UHDBT, an alkyl-hydroxybenzoxythiazole, interact with the Rieske iron-sulfur protein at the center P ubiquinol oxidation pocket in the  $bc_1$  complex (26–30). We thus examined this possible interaction with atovaquone. EPR spectra of the Rieske iron-sulfur center in the purified  $bc_1$  complex from *S. cerevisiae* with and without bound atovaquone are shown in Fig. 3. The ascorbate-reduced Rieske center revealed signals at  $g_z = 2.028$ ,  $g_y = 1.899$ , and  $g_x = 1.75$ . The addition of atovaquone shifted the  $g_z$  and  $g_x$  signals to higher

field,  $g_z = 2.034$  and  $g_x = 1.76$ , whereas the  $g_y$  component showed a lower value,  $g_y = 1.888$ . A shift of the  $g$  value of 0.01, as in the case for the  $g_y$  signal, is  $\sim 21$  Gauss. This corresponds to one times the complete line width of the signal. Atovaquone had almost the same effects on the Rieske EPR spectrum as stigmatellin, although the effects of stigmatellin were more pronounced in the  $g_x$  region. In the bovine  $bc_1$  complex, UHDBT resulted in almost the same  $g$  values as observed for atovaquone in the yeast enzyme (27), and the data are similar to those published for a hydroxynaphthoquinone bound to the Rieske protein in the  $bc_1$  complex from a photosynthetic bacteria (28, 29).

We also tested the effect of atovaquone on the midpoint potential of the Rieske iron-sulfur cluster. The reduction status of the iron-sulfur cluster of the yeast  $bc_1$  complex was monitored by CD spectroscopy as the applied redox potential was varied (Fig. 4). In the absence of inhibitors, the midpoint potential determined from these titrations was 285 mV. This value is identical to that previously obtained for the yeast Rieske protein (20) and also identical to that for the bovine heart Rieske protein (27). In the presence of atovaquone, the midpoint potential of the Rieske iron-sulfur cluster increased from 285 to 385 mV. Due to scatter in the data at low potentials, this value may be as low as 370 mV. This indicates that atovaquone binds  $\sim 50$ -fold more tightly when the Rieske center is reduced. By way of comparison, with nonyl-HDBT, an analog of UHDBT, the midpoint potential increased from 285 to  $350 \pm 12$  mV, similar to the effect of UHDBT on the midpoint potential of the bovine  $bc_1$  complex (27).

**Docking of Atovaquone in the Yeast  $bc_1$  Complex**—An energy-minimized structure of atovaquone was docked in the ubiquinol oxidation pocket at center P using the coordinates of the yeast

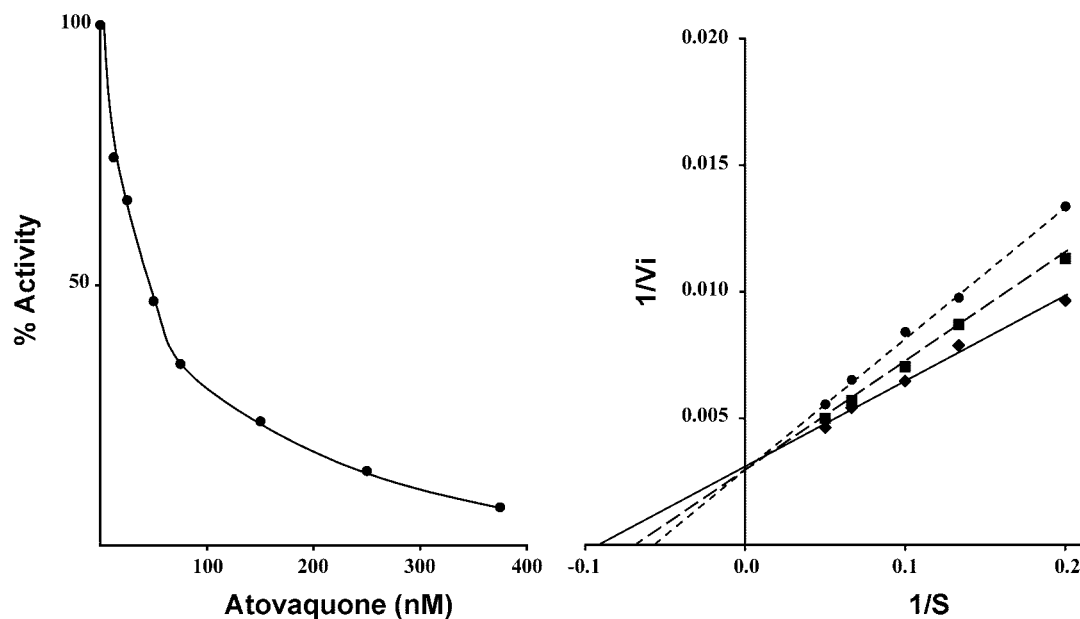


FIG. 2. **Inhibition of yeast cytochrome  $bc_1$  complex by atovaquone.** In the *left panel* cytochrome  $c$  reductase activity of purified yeast  $bc_1$  complex was measured in the presence of varying amounts of atovaquone. In the absence of inhibitor,  $K_{cat} = 130 \text{ s}^{-1}$ . The *right panel* shows reciprocal plots of cytochrome  $c$  reductase activity initial velocity ( $1/\text{s}^{-1}$ ) versus substrate concentration ( $1/\mu\text{M}$ ) measured in the absence of atovaquone (*diamonds*), with 20 nM (*squares*) and with 40 nM (*circles*) atovaquone.

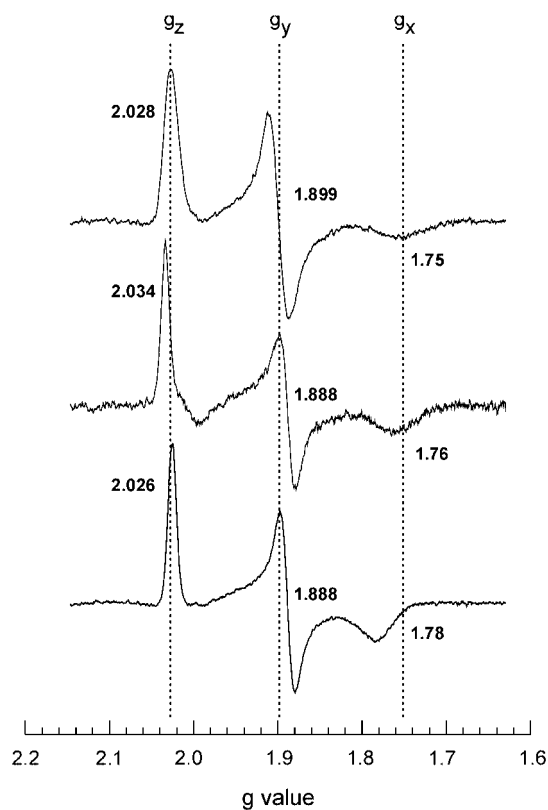


FIG. 3. **Effect of atovaquone on the EPR spectrum of the yeast Rieske iron-sulfur cluster.** The *top spectrum* is of the Rieske iron-sulfur center in the  $bc_1$  complex without inhibitor, the *middle spectrum* is in the presence of atovaquone, and the *bottom spectrum* is in the presence of stigmatellin. The *dashed lines* are drawn through the indicated resonance peaks in the control spectrum to emphasize the shifts of the  $g_x$ ,  $g_y$ , and  $g_z$  signals as a result of inhibitor binding.

$bc_1$  complex and is shown in Fig. 5. In this structure, the naphthoquinone ring of the atovaquone was positioned 2.6 Å deeper than the stigmatellin ring system in order to obtain maximum interaction between the minimized ligand and the

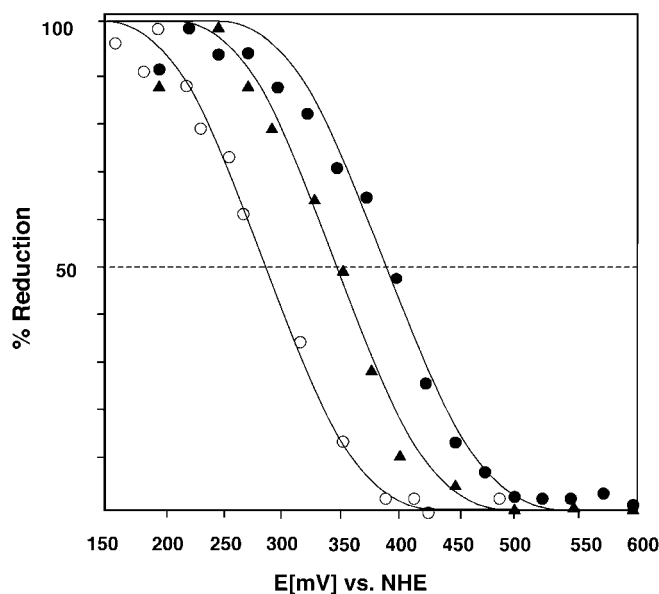
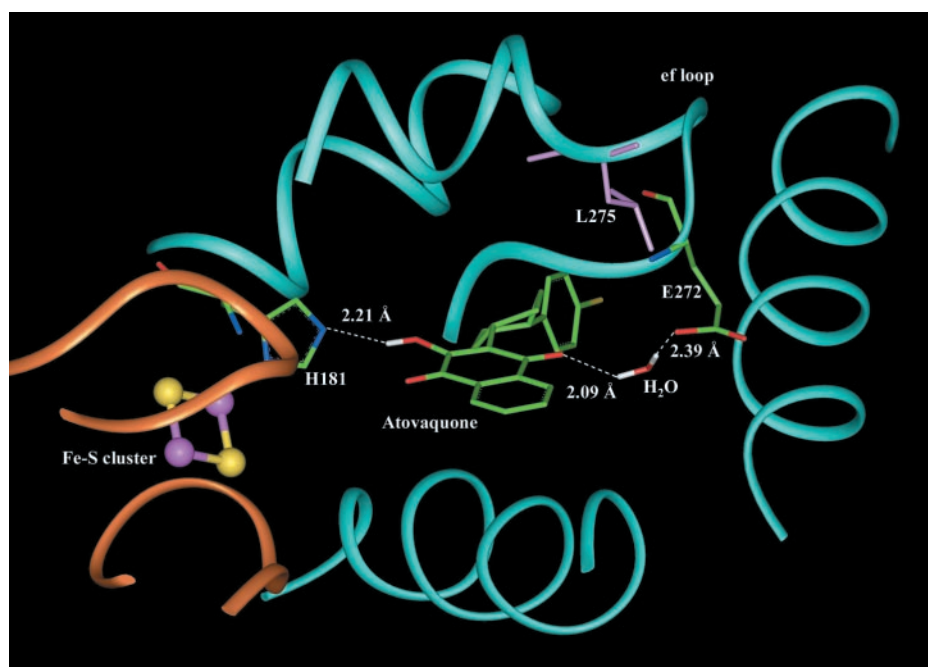


FIG. 4. **Effect of atovaquone and nonyl-HDBT on the midpoint potential of the Rieske iron-sulfur protein.** The redox status of the Rieske iron-sulfur cluster in isolated  $bc_1$  complex was monitored by CD spectroscopy during potentiometric titrations. Titrations were performed in the absence of inhibitor (*open circles*), in the presence of nonyl-HDBT (*solid triangles*), and in the presence of atovaquone (*solid circles*). The amplitude of the CD signals at 500 nm of the full reduced clusters were 1.1, 0.6, and 0.7 millidegrees in the absence of inhibitor, in the presence of nonyl-HDBT, and in the presence of atovaquone, respectively. *NHE*, normal hydrogen electrode.

pocket. As viewed from the naphthoquinone ring and compared with the lowest energy conformation in the unbound form, the cyclohexyl ring rotates 47° clockwise around the bond to the naphthoquinone ring, and the chlorophenyl ring rotates 32° clockwise around the bond to the cyclohexyl ring. These rotational changes involve very little change in conformational energy, which is reasonable, since any such change would have to be compensated for by an increased cost in binding energy.

Notably, the hydroxyl group of the hydroxynaphthoquinone

**FIG. 5. Energy-minimized structure of atovaquone binding in the ubiquinol oxidation pocket at center P of the yeast *bc*<sub>1</sub> complex.** Cytochrome *b* is shown in cyan, and a portion of the Rieske iron-sulfur protein is shown in gold. The iron-sulfur cluster is at the lower left, with iron and sulfur atoms colored purple and yellow, respectively. The C helix of cytochrome *b* is shown extending vertically on the right, and the cd1 helix is shown across the bottom of the binding pocket. Leu<sup>275</sup> and Glu<sup>272</sup> in the ef loop of cytochrome *b* are also shown. Atovaquone is hydrogen-bonded to His<sup>181</sup> of the Rieske protein and to a bound water that forms a bridge to Glu<sup>272</sup> through a second hydrogen bond. The hydroxynaphthoquinone ring is toward the front, and the chlorophenyl ring extends to the rear. The carbon atoms in atovaquone, His<sup>181</sup>, and Glu<sup>272</sup> are green, oxygen atoms are red, nitrogen atoms are blue, and hydrogen atoms are white. Leu<sup>275</sup> is purple.



binds via a hydrogen bond to the nitrogen of His<sup>181</sup> of the Rieske protein. On the opposite side of the ring system, atovaquone interacts with Glu<sup>272</sup> of cytochrome *b* with the carbonyl group at position 4 on the quinone ring. A survey of ~60 protein crystal structures at 2.0 Å or better resolution in the Atlas of Side-chain and Main-chain Hydrogen Bonds (available on the World Wide Web at [www.biochem.ucl.ac.uk/~mcdonald/atlas/glu.html](http://www.biochem.ucl.ac.uk/~mcdonald/atlas/glu.html)) indicates that the side chains of glutamic acid residues are usually not proton donors, due to the low  $pK_a$  of the carboxyl group (see also Ref. 31). In a few cases (32, 33), the  $pK_a$  of glutamic acid residues has been reported as higher when stabilized by a proximal network of coupled aspartic and glutamic residues. Since the closest aspartic acid in cytochrome *b* is 10 Å away from Glu<sup>272</sup>, we ruled out the protonation of its carboxyl group and assumed that Glu<sup>272</sup> is a proton acceptor. Therefore, in order to allow the quinone carbonyl-glutamate carboxyl interaction, a molecule of water was added, and the side chain of Glu<sup>272</sup> was rotated ~180°. This rotation mimics that recently found in the crystal structure of the HDBT-bound yeast *bc*<sub>1</sub> complex (34). After energy minimization, the distance between the hydroxyl group of the atovaquone and the His<sup>181</sup> is 2.21 Å, which is a weaker hydrogen bond than the 1.75 Å found with stigmatellin. This is consistent with the smaller shift in midpoint potential that results from atovaquone binding compared with stigmatellin binding.

As a control to test the importance of the hydroxyl group in docking of atovaquone into the center P site, we removed the hydroxyl group from atovaquone and repeated the molecular modeling. This resulted in atovaquone moving away from the iron-sulfur protein and an increase in the nonbonding interaction energy of 14–54 kcal/mol, depending on the degree of internal strain on the ligand. These changes confirm the importance of the hydroxyl group in atovaquone binding to the ubiquinol oxidation pocket at center P and are consistent with the effects of atovaquone on the Rieske protein and the location of the ligand in the HDBT-bound yeast *bc*<sub>1</sub> complex (34).

**Molecular Basis for Atovaquone Sensitivity**—In order to evaluate the potency of atovaquone on the *bc*<sub>1</sub> complexes of fungi and protozoan parasites relative to the mammalian enzyme, the inhibitory effects of atovaquone on *bc*<sub>1</sub> complexes from yeast and beef heart mitochondria were measured (Fig. 6). Whereas the yeast *bc*<sub>1</sub> complex is inhibited with an  $IC_{50} = 50$

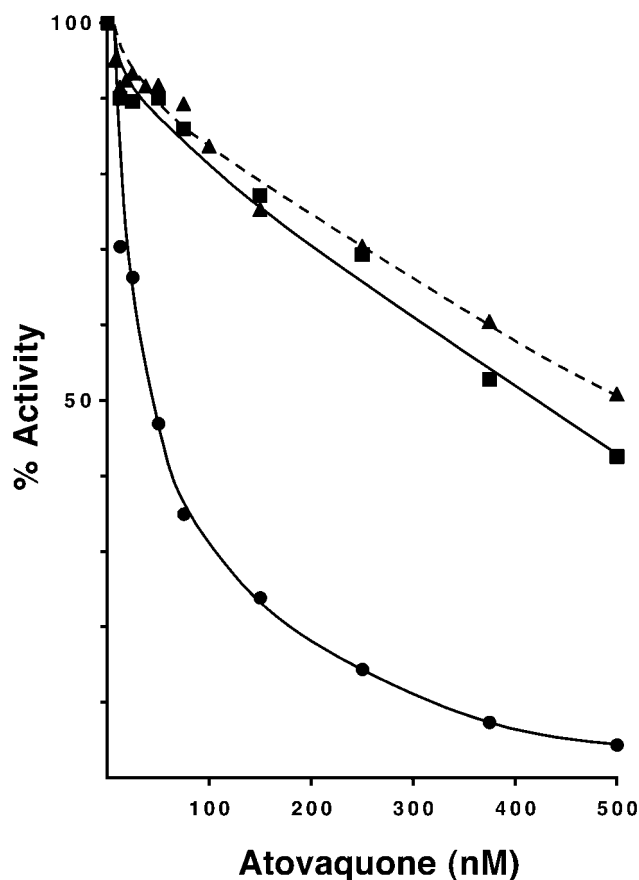


**FIG. 6. Relative efficacies of atovaquone in yeast and bovine *bc*<sub>1</sub> complexes and conferral of resistance to the yeast enzyme with a L275F mutation.** Cytochrome *c* reductase activities of purified *bc*<sub>1</sub> complexes were measured in the presence of increasing concentrations of atovaquone. Activity of the *bc*<sub>1</sub> complex from wild-type yeast (solid circles) in the absence of inhibitor was 170 s<sup>-1</sup>, that of the *bc*<sub>1</sub> complex from the L275F yeast mutant (solid triangles) was 190 s<sup>-1</sup>, and that of the bovine enzyme (solid squares) was 390 s<sup>-1</sup>.

nM, as noted above, under the same assay conditions the bovine enzyme is much less sensitive to the inhibitor, with an  $IC_{50} = 400$  nM.

A ClustalW sequence alignment of the yeast and bovine cytochrome  $b$  subunits around the highly conserved PEWY domain (Fig. 7) showed that one of the amino acids that differs between the two species is at position 275 in the yeast enzyme. This position is occupied by a leucine in the *S. cerevisiae* sequence and a phenylalanine in the bovine sequence. A L275F mutation was thus generated *in silico* and submitted to molecular dynamics and energy minimization. As shown in Fig. 8, replacement of Leu<sup>275</sup> with phenylalanine resulted in significant predicted steric changes, with the appearance of a “bulge” in the atovaquone binding pocket resulting from the increased van der Waals radius of the aromatic ring. We calculated an increased energy cost for atovaquone binding of 16.21 kcal/mol as a result of the phenylalanine for leucine substitution. It is not possible to directly convert the binding energy into a  $K_i$  value, since the units in these force field calculations are arbitrary. However, this calculated change in binding energy from the molecular modeling is qualitatively consistent with the 8-fold increase in apparent  $IC_{50}$  measured on the bovine enzyme.

To further evaluate whether the phenylalanine at position

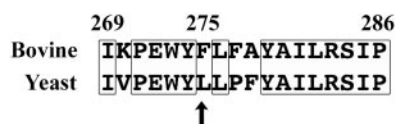


FIG. 7. Amino acid sequence alignment of the conserved 269–286 region of the cytochromes  $b$  of *S. cerevisiae* and *Bos taurus*. The alignment was constructed using ClustalW and yeast numbering. The arrow points to the residues at position 275.

275 in the bovine cytochrome  $b$  is responsible for the relative resistance of that  $bc_1$  complex to atovaquone, we introduced a L275F mutation into the yeast cytochrome  $b$  by biolistic transformation of the mitochondrial genome. We then measured the inhibitory effects of atovaquone on the  $bc_1$  complex isolated from the L275F yeast mutant. As can be seen in Fig. 6, the L275F mutation conferred atovaquone resistance to the yeast enzyme comparable with that of the bovine, raising the  $IC_{50}$  to 500 nM, which would correspond to an apparent  $K_i = 100$  nM. The mutation had no detrimental effect on the cytochrome  $c$  reductase activity of the enzyme from the mutant. From this result, we conclude that the exchange of phenylalanine for leucine at position 275 in cytochrome  $b$  is largely responsible for the differential efficacy of atovaquone in these two species.

#### DISCUSSION

It has been known since the 1940s (2) that hydroxynaphthoquinones inhibit respiration in malarial parasites. Based on changes in the redox poise of the cytochromes in response to atovaquone addition, it was later deduced that its primary site of action in the parasite is the cytochrome  $bc_1$  complex (4). Numerous subsequent studies have assumed that atovaquone interacts with the  $bc_1$  complex and have even attempted to model the ligand into the ubiquinol oxidation pocket (10–13). However, none have investigated the interaction of atovaquone with the purified enzyme or documented its interaction at center P. We are developing the yeast *S. cerevisiae* as a model organism in which to better understand the basis of atovaquone resistance in parasites and pathogenic fungi (15). In the current study, we have characterized the interaction of atovaquone with the yeast  $bc_1$  complex.

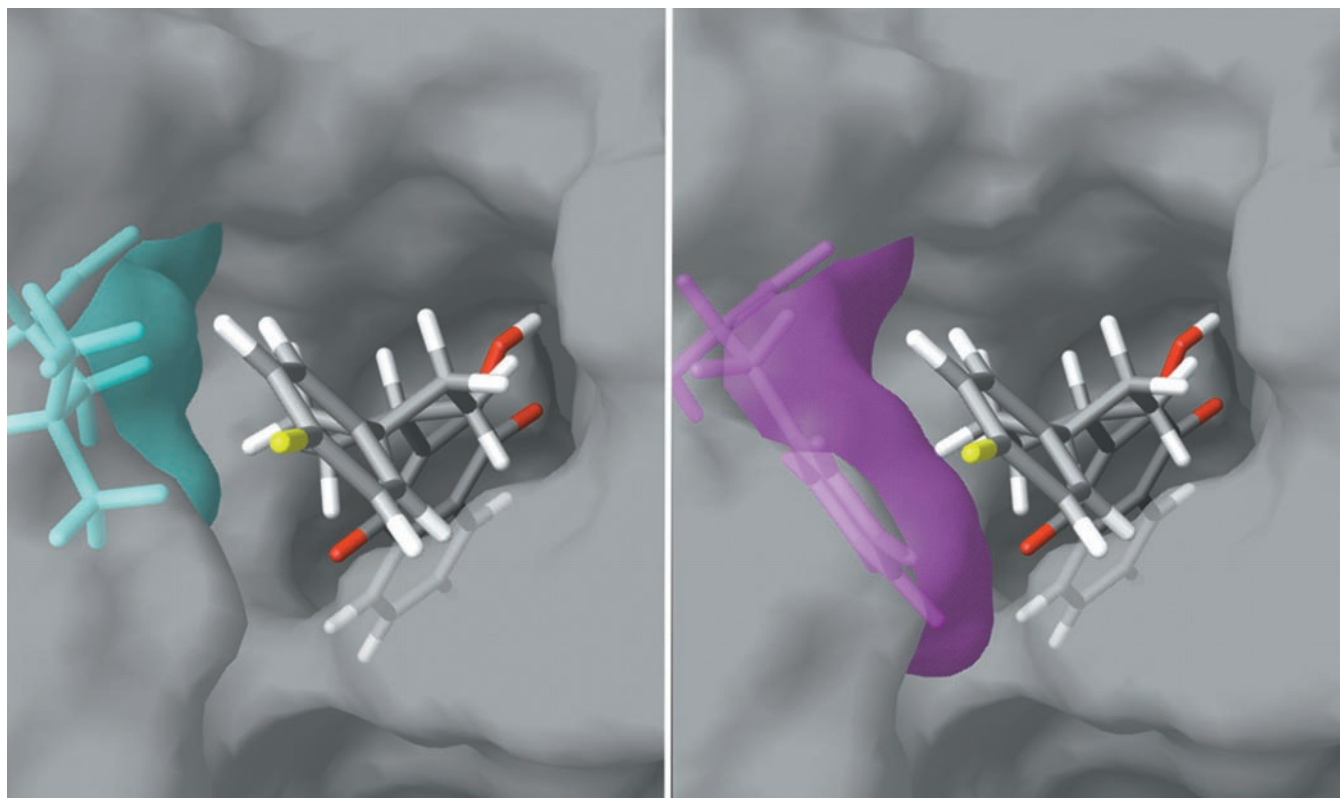


FIG. 8. Views of atovaquone binding in the  $bc_1$  complexes of wild type yeast (left panel) and the L275F mutant (right panel). The images were generated by energy minimization of atovaquone bound to the  $bc_1$  complexes from wild-type yeast and the L275F mutant to illustrate the steric hindrance to atovaquone binding that results from the replacement of leucine by phenylalanine. The blue residue in the left panel is Leu<sup>275</sup>, and the magenta residue in the right panel is Phe<sup>275</sup>, both are shown with their associated van der Waals radii. The chlorine atom on atovaquone is yellow-green, oxygen atoms are red, and hydrogen atoms are white. The view is from the bottom of the ubiquinol-binding pocket. Atovaquone is shown with the chlorophenyl group toward the front and the naphthoquinone ring system to the rear. His<sup>181</sup> of the Rieske protein and Glu<sup>272</sup> of cytochrome  $b$  that are bridged by the hydroxynaphthoquinone ring would be located to the rear from this perspective. The figure was generated using GRASP software.

Like stigmatellin and methoxylacrylates such as myxothiazol, atovaquone is a competitive inhibitor that specifically targets the ubiquinol oxidation pocket at center P of the *bc*<sub>1</sub> complex. The effects of atovaquone on the *bc*<sub>1</sub> complex, notably its effects on the Rieske iron-sulfur center, are most like those of another hydroxynaphthoquinone and UHDBT (27–29). The magnetic field shifts in the EPR spectrum reflect a change in the electronic environment surrounding the 2Fe-2S cluster as a result of the ligand binding. The changes in midpoint potential indicate ~50-fold tighter binding of the ligand when the Rieske center is reduced. Together, these results indicate that atovaquone binds to the ubiquinol oxidation pocket when the soluble domain of the Rieske protein is proximal to cytochrome *b* and that it interacts directly with the iron-sulfur protein.

We used the biochemical and spectroscopic results to model atovaquone into the ubiquinol oxidation pocket of the yeast *bc*<sub>1</sub> complex. After computing an energy-minimized structure with the ligand bound to the protein, we found that atovaquone forms a hydrogen bond between the hydroxyl group on the naphthoquinone ring of the inhibitor and His<sup>181</sup> of the iron-sulfur protein. This structure satisfied the requirement that the ligand must interact with the iron-sulfur protein and accounted for the lowering of the midpoint potential of the Rieske iron-sulfur cluster. However, it did not resolve the issue of how the quinone carbonyl group of the naphthoquinone ring, which was oriented toward Glu<sup>272</sup> of cytochrome *b*, could form a hydrogen bond to the carboxylate anion. This problem was solved when a bound water molecule was included to allow a second hydrogen bond similar to that observed in the crystal structure of the HDBT-liganded yeast *bc*<sub>1</sub> complex (34). The only difference between the water-mediated hydrogen bond in the structure modeled here and the HDBT-liganded structure is that we used the carboxyl group of the glutamate rather than the backbone nitrogen as the hydrogen acceptor. The resulting modeled structure accounted for the enzymatic and spectroscopic results and was more stable than the structure lacking the water-mediated hydrogen bond. This computed structure differs significantly from two previously postulated structures for atovaquone bound to the *bc*<sub>1</sub> complex (12, 13). In those structures, the hydroxyl group of atovaquone was oriented toward Glu<sup>272</sup> in both cases, and one of the structures failed to account for atovaquone interaction with the Rieske protein (13).

In order to be effective therapeutically, atovaquone must exhibit some preferential efficacy of inhibition of respiration in the targeted pathogen compared with the mammalian host. We have used the yeast and bovine *bc*<sub>1</sub> complexes as surrogates to model the interaction of atovaquone with parasite, fungal, and human enzymes. The cytochrome *b* sequence of yeast is ~40 and 60% identical to those of *Plasmodium* and *P. carinii*, respectively, and that of the bovine protein is 80% identical to the human protein. The IC<sub>50</sub> measurements showed that atovaquone is about 8 times more potent with the yeast *bc*<sub>1</sub> complex than with the bovine enzyme.

The computed structure of atovaquone bound to the ubiquinol oxidation pocket provided a potential insight into the structural basis for the differential efficacy of atovaquone with yeast and bovine *bc*<sub>1</sub> complexes. The ef loop of cytochrome *b* is a conserved domain containing residues in close contact to the atovaquone-binding pocket. Notably, the residue at position 275 in this loop is a leucine in *S. cerevisiae* and *P. carinii* cytochromes *b* but is substituted with a phenylalanine in both the bovine and human proteins. When a L275F mutation was modeled into the computed structure of the atovaquone bound

enzyme, it resulted in a steric constraint to atovaquone binding and a predicted decrease in the affinity of the inhibitor to the binding pocket. When the mutation was introduced into the yeast cytochrome *b* gene, the sensitivity of the *bc*<sub>1</sub> complex to atovaquone was reduced to a level similar to that of the bovine enzyme, thus confirming *in vivo* what was predicted *in silico*. Whereas other structural features of cytochrome *b* may also contribute to the differential sensitivity of the species to this drug, the residue at position 275 appears to be a key determinant of efficacy of ligand binding to the *bc*<sub>1</sub> complex. The L275F mutation also confers resistance of *S. cerevisiae* to myxothiazol, another inhibitor that binds to the ubiquinol oxidation pocket at center P in the *bc*<sub>1</sub> complex (35).

*Acknowledgments*—We thank Dr. Thomas Link for use of the CD spectrometer and Dr. Uli Brandt for the use of laboratory facilities.

#### REFERENCES

1. Trumppower, B. L., and Gennis, R. B. (1994) *Annu. Rev. Biochem.* **63**, 675–716
2. Wendel, W. B. (1946) *Fed. Proc.* **5**, 406–407
3. Hudson, T., Dickins, M., Ginger, C. D., Gutteridge, W. E., Holdich, T., Hutchinson, D. B. A., Pudney, M., Randall, A. W., and Latter, V. S. (1991) *Drugs Exp. Clin. Res.* **17**, 427–435
4. Fry, M., and Pudney, M. (1992) *Biochem. Pharmacol.* **43**, 1545–1553
5. Araujo, F. G., Huskinson, J., and Remington, J. S. (1991) *Antimicrob. Agents Chemother.* **35**, 293–299
6. Boehm P., Cooper, K., Hudson, A. T., Elphick, J. P., and McHardy, N. (1981) *J. Med. Chem.* **24**, 295–299
7. Hughes, W. T., and Oz, H. S. (1995) *J. Infect. Dis.* **172**, 1042–1046
8. Hughes, W. T., Gray, V. L., Gutteridge, W. E., Latter, V. S., and Pudney, M. (1990) *Antimicrob. Agents Chemother.* **34**, 225–228
9. Walker, D., Wakefield, A., Dohn, M., Miller, R., Baughman, R., Hossler, P., Bartlett, M., Smith, J., Kazanjian, P., and Meshnick, S. R. (1998) *J. Infect. Dis.* **178**, 1767–1775
10. Srivastava, I. K., Morrissey, J. M., Darrouzet, E., Daldal, F., and Vaidya, A. B. (1999) *Mol. Microbiol.* **33**, 704–711
11. Syafruddin, D., Siregar, J. E., and Marzuki, S. (1999) *Mol. Biochem. Parasitol.* **104**, 185–194
12. McFadden, D. C., Tomavo, S., Berry, E. A., and Boothroyd, J. C. (2000) *Mol. Biochem. Parasitol.* **108**, 1–12
13. Korsinczyk, M., Chen, N., Kotecka, B., Saul, A., Rieckmann, K., and Cheng, Q. (2000) *Antimicrob. Agents Chemother.* **44**, 2100–2108
14. Kazanjian, P., Armstrong, W., Hossler, P. A., Huang, L., Beard, C. B., Carter, J., Crane, L., Duchin, J., Burman, W., Richardson, J., and Meshnick, S. R. (2001) *J. Infect. Dis.* **183**, 819–822
15. Hill, P., Kessl, J., Fisher, N., Meshnick, S., Trumppower, B. L., and Meunier, B. (2003) *Antimicrobiol. Agents Chemother.*, in press
16. Hunte, C., Koepke, J., Lange, C., Rossmannith, T., and Mitchel, H. (2000) *Structure* **8**, 669–684
17. Snyder, C. H., and Trumppower, B. L. (1999) *J. Biol. Chem.* **274**, 31209–31216
18. Ljungdahl, P. O., Pennoyer, J. D., Robertson, D., and Trumppower, B. L. (1987) *Biochim. Biophys. Acta* **891**, 227–242
19. Cheng, Y. C., and Prusoff, W. H. (1973) *Biochem. Pharmacol.* **22**, 3099–30108
20. Denke, E., Merbitz-Zahradnik, T., Hatzfeld, O. M., Snyder, C. H., Link, T. A., and Trumppower, B. L. (1998) *J. Biol. Chem.* **273**, 9085–9093
21. Hehre, W. J., Yu, J., Klunzinger, P. E., and Lou, L. (1998) *A Brief Guide to Molecular Mechanics and Quantum Chemical Calculations*, pp. 7–35, Wavefunction, Inc., Irvine, CA
22. Nose, S. (1984) *J. Chem. Phys.* **81**, 511–519
23. Jacobs, D. A. H. (1977) *The State of the Art in Numerical Analysis*, pp. 256–258, Academic Press, London
24. Fletcher, R. (1987) *Practical Methods of Optimization*, pp. 54–57, Academic Press, Inc., New York
25. Kunze, B., Kemmer, T., Höfle, G., and Reichenbach, H. (1984) *J. Antibiot.* **37**, 454
26. Covian, R. Pardon, J. P., and Moreno Sanchez, R. (2002) *J. Biol. Chem.* **277**, 48449–48455
27. Bowyer, J. R., Edwards, C. A., Ohnishi, T., and Trumppower, B. L. (1982) *J. Biol. Chem.* **257**, 8321–8330
28. Bowyer, J. R., Dutton, P. L., Prince, R. C., and Crofts, A. R. (1980) *Biochim. Biophys. Acta* **592**, 445–460
29. Matsuura, K., Bowyer, J. R., Ohnishi, T., and Dutton, P. L. (1983) *J. Biol. Chem.* **258**, 1571–1579
30. von Jagow, G., and Ohnishi, T. (1985) *FEBS Lett.* **185**, 311–315
31. McDonald, E. K., and Thornton, J. M. (1994) *J. Mol. Biol.* **238**, 777–793
32. Maroti, P., Hanson, D. K., Schiffer, M., and Sebban, P. (1995) *Nat. Struct. Biol.* **2**, 1057–1059
33. Sampogna, R. V., and Honig, B. (1996) *Biophys. J.* **71**, 1165–1171
34. Palsdottir, H., Gomez Lojero, C., Trumppower, B. L., and Hunte, C., (2003) *J. Biol. Chem.* **278**, 31303–31311
35. Di Rago, J. P., Coppée, J. Y., and Colson, A. M. (1989) *J. Biol. Chem.* **264**, 14543–14548